Energy Reports 8 (2022) 4453–4460

Contents lists available at ScienceDirect

Energy Reports

journal homepage: www.elsevier.com/locate/egyr

Research paper

Enhancement of novel $NaZnBr_3$ perovskite for solar cells application

Moses E. Emetere [a,*], Oluwaseyi O. Bello [b], S.A. Afolalu [c]

[a] Department of Mechanical Engineering Science, University of Johannesburg, South Africa
[b] Physics Department, Covenant University Canaanland, P.M.B 1023, Ota, Nigeria
[c] Department of Mechanical Engineering, Afe Babalola University, Nigeria

ARTICLE INFO

Article history:
Received 29 October 2021
Received in revised form 13 January 2022
Accepted 11 March 2022
Available online xxxx

Keywords:
Solar cell
Inorganic perovskite
Lead-free perovskite
Power conversion efficiency (PCE)
Current density
Voltage

ABSTRACT

The efficiencies of lead-based inorganic and organic–inorganic hybrid perovskite solar cells have been approaching 25% in recent years. Their major challenges include instability problems and their possible long term health hazards. In response to this, there has been a growth in research into lead-free inorganic perovskites. This research proposed that structural modifications of perovskite using copper and silver dopants be used as a unique technique for enhancing the efficiency of novel $NaZnBr_3$. The optical, microstructural, electronic, and crystalline characterization was carried out using Ultraviolet–Visible (UV–VIS) spectroscopy, Scanning Electron Microscopy (SEM), SCAPS-1D, and X-ray Diffractometry (XRD) respectively. $NaZnBr_3$ had an efficiency of 0.88% at 100 μm, with a band gap of 3.1 eV. This efficiency improves to 9.33% with silver additive with a bandgap of 1.65 eV. Pure $NaZnBr_3$ is found to be a p–n type semiconductor via its flat band potential, while doped $NaZnBr_3$ are shown to be p-type semiconductors. Silver is concluded to be the better dopant, although both dopants increased the efficiency and show higher doping densities and external quantum efficiencies than pure $NaZnBr_3$. It was reported that the crystallographic and microstructural structure of the perovskite plays a significant role in the optimization or modification of the efficiency of the novel $NaZnBr_3$ perovskite. It is recommended that $NaZnBr_3$ be researched further using different synthetic routes and experimental electronic measurement.

1. Introduction

Perovskites, which are a class of compound with the general formula ABX3, are a promising replacement for silicon in solar cells. 'A' & 'B' are cations of dissimilar bulks, 'A' being normally larger than 'B', and 'X' being an anion, which can be oxygen or a halogen. Perovskites have been shown to have excellent photoelectric properties. For example, they have high optical absorption coefficients and lower exciton binding energy (Zhou et al., 2018). They also have conducting, superconducting, and piezoelectric properties (Ahmed et al., 2015). These properties make them suitable for use in several electrical devices, particularly those that require semiconductors (Elumalai et al., 2016). The high absorption coefficients of perovskites mentioned earlier indicates that they are possible replacements for silicon in the role of the light absorbing layer in solar cells. One of their advantages in this regard are the lower costs involved in producing them, as well as their impressive efficiency (Roy et al., 2020). Perovskites are also useful as hole transport layers in other types of solar cells (Rahman et al., 2018).

The best performing perovskite solar cells (PSCs) have been the lead-based perovskites of the inorganic and organic–inorganic hybrid types. The highest efficiency of these kinds of solar cells is a perovskite/silicon tandem cell, with an efficiency of 25.2% (Sahli et al., 2018). These lead based perovskite solar cells (PSCs) have problems of instability and toxicity. Lead is toxic, and has been banned from a variety of uses that would lead to it being ingested or absorbed into humans. The problem of instability leads to the fear that a possible large-scale manufacture of these cells could lead to environmental and health disasters in both human and non-human life and ecosystems (Zhou et al., 2018). It would therefore be prudent to find replacements that could give a similar or better performance without the risk of toxicity and degradation, and this is why research into lead-free perovskites, particularly the inorganic type, has been picking up over recent years (Roman-Vazquez et al., 2020). The $CsSnI_3$-based lead-free perovskite solar cell has had one of the highest efficiencies of its class at 7.11% (Chen et al., 2019). Its disadvantage is that it is still has instability problems which deteriorate the efficiency. Because of this instability that comes with replacing lead with similar cations such as Tin, there have been attempts to replace lead with two cations (Bi^+ and Bi^{3+}) in "double perovskite" compounds instead (Greul et al., 2017; Shao et al., 2018; Igbari et al., 2019). The chemical formula of such compounds, as postulated by Zhang

* Corresponding author.
E-mail address: emetere@yahoo.com (M.E. Emetere).

https://doi.org/10.1016/j.egyr.2022.03.087

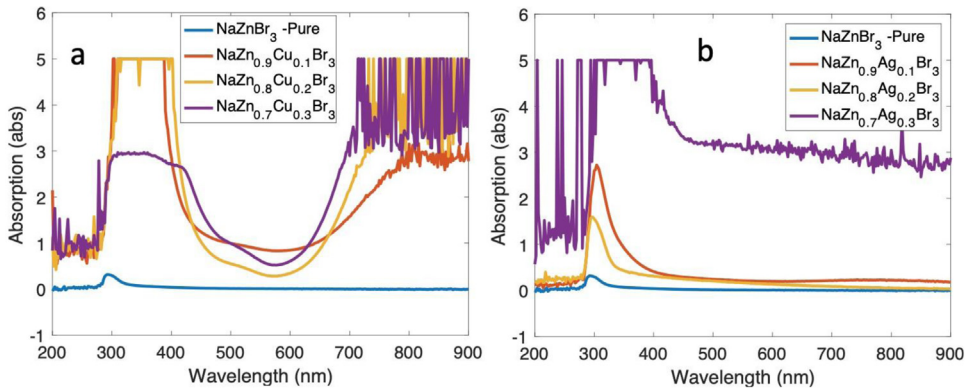

Fig. 1A. (a) UV spectra of pure and Copper doped $NaZnBr_3$ (b) UV spectra of pure and Silver doped $NaZnBr_3$.

et al. (2020) and Zhao et al. (2020), is $A2M^{I}M^{III}X6$ (A=Cs, MA; M^{I}=Ag, Na, K; M^{III}=Sb, Bi; X=Cl, Br, I). The trade-off for gaining stability is a loss in efficiency due to the relatively large band gap of the double perovskites. The $Cs_2AgBiBr_6$ PSCs reported by Wang et al. (2018) had a maximum PCE of 1.37%. The PSC retained more than 90% of that original PCE after storage in air at 7% Relative Humidity for 240 h. The 2.43% PCE of the $Cs_2AgBiBr_6$ based PSCs constructed by Greul et al. (2017) displayed only a 5% decay over a 30 s period, and then reduces to and stabilizes at an efficiency of 1.9%. The reduction in PCE is due to the large band gap of these compounds. The advantage of these double perovskites is their stability, unlike compounds that simply replace lead with similar cations. Their low efficiencies means that one problem (i.e. stability) has been replaced with another (i.e. efficiency), and there is need for perovskites which have the advantage of both efficiency and stability. In this study, $NaZnBr_3$ was synthesized. Separate samples were doped with Copper and Silver. Its band gap was found using UV–Vis analysis and Tauc plots. The information from the UV–Vis analysis was used in SCAPS-1D in order to determine its power conversion efficiency (PCE), as well as to estimate several other parameters such as doping density, external quantum efficiency, and flat band potential in order to determine the overall performance of the simulated solar cell.

2. Method

In order to synthesize pure $NaZnBr_3$, 0.04 moles of NaBr and $ZnBr_2$ were mixed in the ratio 1:1 in a beaker with 50 ml of distilled water to give a clear solution, after which 2 ml from the mixture was collected for UV–Vis analysis. The dissolved $NaZnBr_3$ was then heated at 250 °C for 12 h in order to dry them completely, after which they were put in labeled PET bottles. In the case of the doped samples, the doping compounds ($Cu(NO_3)2$, and $AgNO_3$), were mixed in with the precursors in such a ratio that the molar portion of zinc and the molar portion of the dopant should add up to 0.04. NH_4Br was added to make up for the bromine in the proposed perovskite when the amount of ZnBr is reduced in order to add the dopant. The mixture was then heated to remove the unwanted by-products of the reaction via evaporation. The table for the synthesis in this regard is given in Table 1. The solutions with copper were a blue–green color, while those with silver were clear with a light green precipitate. From the pre-heated mixtures, 2 ml portion was taken for UV–Vis analysis while the rest were dried at by heating at 250 °C for 12 h.

The electrical characterization was performed using SCAPS-1D, which is a windows-based 1- dimensional solar cell capacitance simulator. It simulates profiles such as grading, device architecture, defects, and recombination using Poisson's equation

Table 1
Molar quantities of precursors and dopants.

Compound	NaBr	$ZnBr_2$	$Cu(NO_3)_2$	$AgNO_3$	NH_4Br
$NaZn_{0.9}Cu_{0.1}Br_3$	0.04	0.036	0.004	0	0.008
$NaZn_{0.8}Cu_{0.2}Br_3$	0.04	0.032	0.008	0	0.016
$NaZn_{0.7}Cu_{0.3}Br_3$	0.04	0.028	0.012	0	0.024
$NaZn_{0.9}Ag_{0.1}Br_3$	0.04	0.036	0	0.004	0.008
$NaZn_{0.8}Ag_{0.2}Br_3$	0.04	0.032	0	0.008	0.016
$NaZn_{0.7}Ag_{0.3}Br_3$	0.04	0.028	0	0.012	0.024

(which relates the charge to the electrostatic potential Φ) and the continuity equations for electrons and holes (Niemegeers and Burgelman, 1996). The software, with the input of the band gap and the absorption data from the UV–Vis analysis, was used to find parameters such as diffusion lengths, current density, open circuit voltage, and photo conversion efficiency.

The structure of the perovskite is TiO_2/ZnO/Perovskite/P3HT. The parameters for the simulation used in this research is given in Table 2. The band gaps for the perovskites are given in Table 3.

When the pure and doped samples were dried via heating at 250 °C for 12 h. It was observed that the resulting samples are deliquescence by nature. After several times of drying and the substance keeps absorbing moisture from the atmosphere and forms a solution, it was mixed with the powder of a native rice seed so that it can be handy to characterized further. The rice grain samples were milled to <20 μm using mechanical grinding mill. Rice was used because of the presence of very low mineral elements (Wannee and Arporn, 2014). The rice that was used was a local known as 'Ofada'. Usikalu et al. (2017) had characterized this rice and found that it has 8805.5 ± 221, 276.5 ± 32, 3704.5±39, 212±8, 110.5 ± 8, 125.5 ± 7, 14.5 ± 1 and 44.5 ± 4 ppm for P, Cl, K, Ca, Mn, Fe, Cu and Zn respectively. The mixture of the $NaZnBr_3$ and rice powder was done in ratio 1:3. The microstructural and morphology of the novel $NaZnBr_3$ perovskite was characterized using scanning electron microscope (SEM) analysis and the crystalline nature of the compound was investigated using the X-ray diffraction (XRD).

3. Results and discussion

Fig. 1A shows the UV–Vis graphs of Copper and Silver doped $NaZnBr_3$ respectively. The doped samples have significantly higher absorptions than the pure sample. The peak of the pure sample is in the 280 nm to 320 nm range. Fig. 1(a) follows the same general pattern, with two peaks; a narrower n–n^* transition with a peak followed by a wider σ–σ^* transition peak. For the shorter peak, Fig. 4 displays a shorter peak for the n–n^* transition in the case of the highest doped sample, while

Table 2
Parameters for Simulated Solar Cell Structure (Rahman et al., 2019).

	ZnO	TiO_2	Perovskite	P3HT
Thickness μm	80	80	100/10/0.001/0.01	65
Band gap (eV)	3.2	3.3	–	1.8
Affinity (eV)	4.1	4.2	4.19	3.9
Dielectricpermittivity	8.1	10	5.8	3
Conduction Band (cm^{-3})	4×10^{-18}	2.5×10^{18}	1×10^{16}	1×10^{20}
Valence Band (cm^{-3})	1×10^{-18}	1×10^{18}	1×10^{16}	1×10^{20}
Electron mobility (cm^2/V s)	300	0.1	20	1×10^{-4}
Hole mobility (cm^2/V s)	1	0.1	20	1×10^{-4}
Acceptorconcentration (cm^{-3})	0	0	1×10^{19}	–
Donor concentration (cm^{-3})	1×10^{19}	1×10^{19}	1×10^{19}	1×10^{16}

Table 3
Band gaps, pH, and power conversion efficiencies of pure, additive modified, and doped $NaZnBr_3$ at different thicknesses.

Material	pH	Band Gap	Efficiency (%) at 100 μm	Efficiency (%) at 10 μm	Efficiency (%) at 1 nm	Efficiency (%) at 10 nm
$NaZnBr_3$	5.61	3.1	0.88	0.86	1.92	1.91
$NaZn_{0.9}Cu_{0.1}Br_3$	4.51	1.77	4.35	4.08	1.95	2.15
$NaZn_{0.8}Cu_{0.2}Br_3$	4.38	2.06	8.33	8.26	3.33	X
$NaZn_{0.7}Cu_{0.3}Br_3$	4.33	1.76	8.33	8.26	2.08	3.331
$NaZn_{0.9}Ag_{0.1}Br_3$	5.88	2.95	9.28	7.82	1.93	1.97
$NaZn_{0.8}Ag_{0.2}Br_3$	5.88	2.39	8.08	6.86	1.92	1.92
$NaZn_{0.7}Ag_{0.3}Br_3$	5.86	1.65	9.33	8.11	2.02	2.80

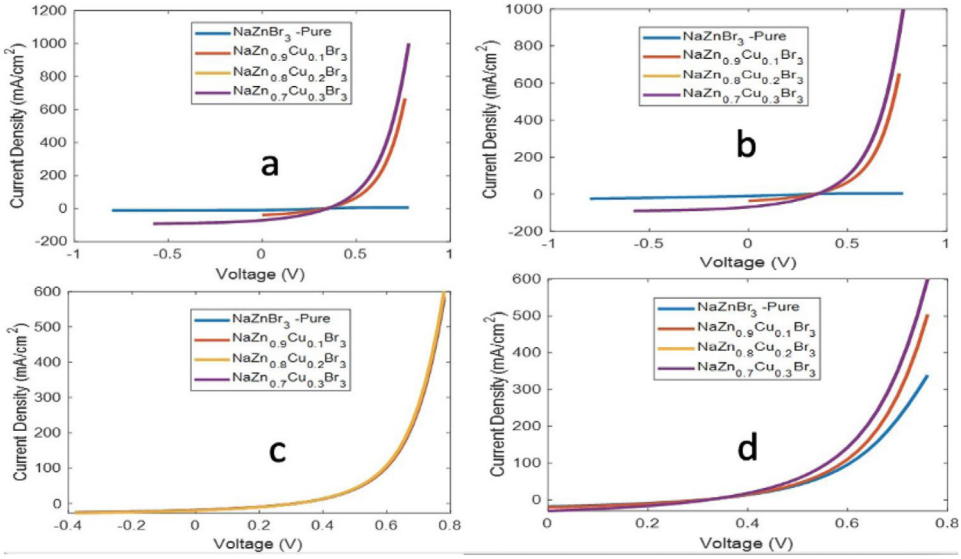

Fig. 1B. JV curves of simulated $NaZnBr_3$-based solar cells with and without copper dopant with perovskite thicknesses (a) 100 μm, (b) 10 μm, (c) 1 nm, (d) 10 nm.

having the highest σ–σ^* transition peak. The band gap of pure $NaZnBr_3$ is 3.1 eV. This figure is greatly reduced with the addition of dopants in smaller doses, but rises slightly with dosage, the highest among the doped samples being $NaZn_{0.7}Cu_{0.3}Br_3$ with 1.76 eV, significantly lower and somewhat advantageous for solar cell usage.

Only one peak appears for the various Silver doped samples in Fig. 1A(b). The wavelength is between 280 nm and 470 nm for the widest peaks. This widest peak belongs to the $NaZnBr_3$with the highest amount of silver dopant. The rise in peaks and their broadening is most likely due to the Silver, which has its peak between 350 nm and 700 nm (Dengler et al., 2012). Their band gaps are higher than those doped with copper, but all lower by at least 0.185 eV, and still in semiconductor range (Fig. 2).

Fig. 1B shows the JV graphs of copper doped $NaZnBr_3$. The pure sample itself has a very poor performance, with an efficiency of 0.88%, a performance reflected in the near horizontal graph that starts with a very low Jsc. The addition of copper dopants greatly increased the efficiency. They start at higher Jsc, and have better efficiencies, especially in both micrometer thicknesses, peaking at 8.33% for $NaZn_{0.7}Cu_{0.3}Br_3$ based cells. Their efficiencies drop off at the nanometer ranges, although they do not start converging immediately. They are still distinct at 10 nm. This might be due to the strong effects of copper doping (Ramyadevi et al., 2011).

The doping, although for one of the doped sample graphs, this range is extended at 10 μm. The graphs, however, narrow and converge at the nanometer range, as it is with the others.

Fig. 3 displays the Mott Schottky Curves of pure and Cooper doped $NaZnBr_3$. The curve for pure $NaZnBr_3$ at 100 μm is strange in that it has two lowest points. It is an oddly shaped Boltzmann curve, with each depression in the positive and negative section of the V axis respectively. This indicates that it is a p–n

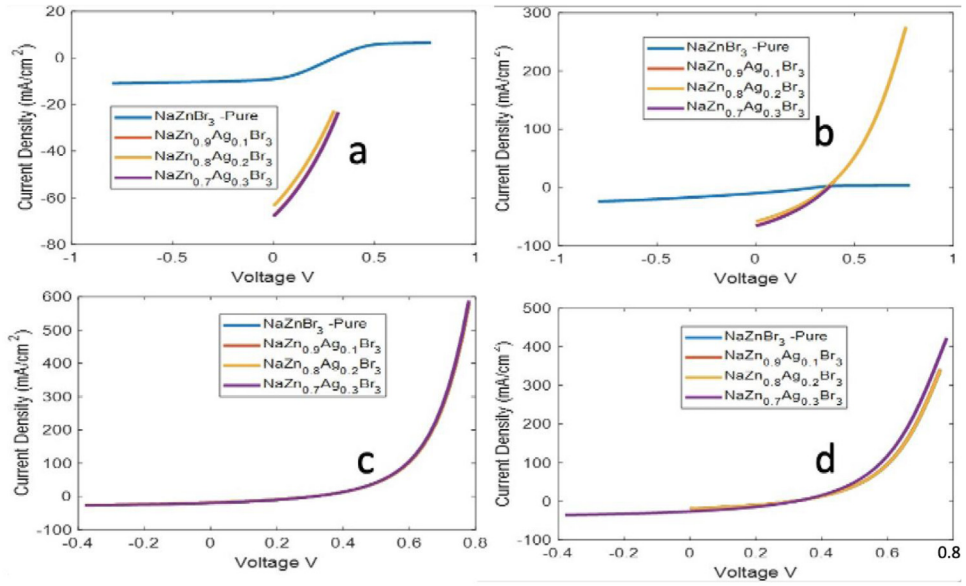

Fig. 2. JV curves of simulated $NaZnBr_3$-based solar cells with and without silver dopant with perovskite thicknesses (a) 100 μm, (b) 10 μm, (c) 1 nm, (d) 10 nm.

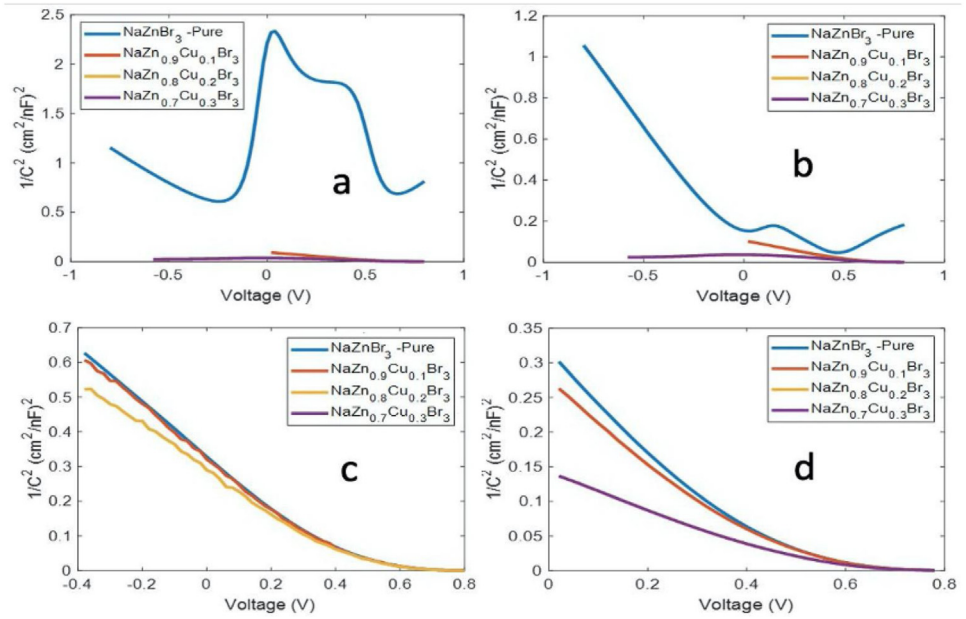

Fig. 3. Mott Schottky curves of simulated $NaZnBr_3$-based solar cells with and without Copper dopant with perovskite thicknesses (a) 100 μm, (b) 10 μm, (c) 1 nm, (d) 10 nm.

semiconductor, making it suitable for heterojunction solar cells (Swain et al., 2018). It has a slightly higher n-bias due to the depression in the n- side of the V axis being the lowest vertically. This phenomenon is rapidly suppressed at lower thicknesses. Its slopes at 100 μm and at 10 μm also indicate a very low doping density, and hence a lower performance than the Cooper doped versions, where this p–n semiconductor becomes simply a p-type semiconductor and have smaller slopes. The effects of the Copper dopants are not eliminated at the nanoscale. Fig. 4 shows a positive influence of copper on the $NaZnBr_3$ in terms of doping density, Vfb and hence solar cell performance. The same disappearance of the p–n semiconductor phenomenon is observed for the pure sample as the thickness decreases, and the homogenization at the nanoscale is not complete due to the effect of silver.

Pure $NaZnBr_3$ has less EQE than its copper doped counterparts (Fig. 5), with several peaks which seem to be smoothed over by the copper doping, and mostly homogenized at the nanoscale. This effect is still present when doped with silver (Fig. 6), but less pronounced, with a particular concentration of dopant having less EQE than the rest in both micrometer scales, and breaking off from the rest at 680 nm. This indicates a lesser PV performance. The curves still homogenize at the nanoscale.

The n–n* transition for the highest doped $NaZnBr_3$ is between 280 nm to 580 nm, while the largest σ–σ^* transition is between 600 nm and 900 nm. σ–σ^* peaks are most likely caused by the

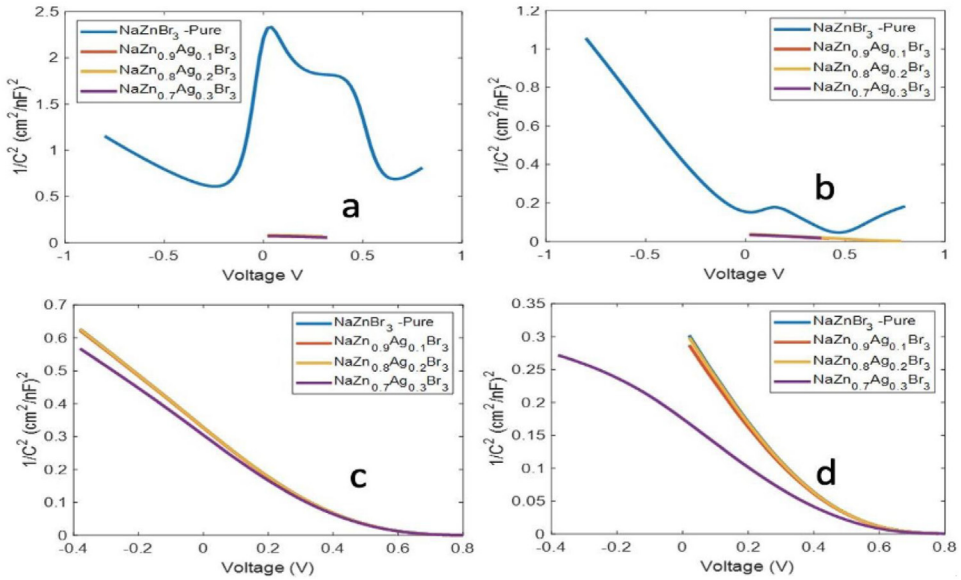

Fig. 4. Mott Schottky curves of simulated $NaZnBr_3$-based solar cells with and without silver dopant with perovskite thicknesses (a) 100 μm, (b) 10 μm, (c) 1 nm, (d) 10 nm.

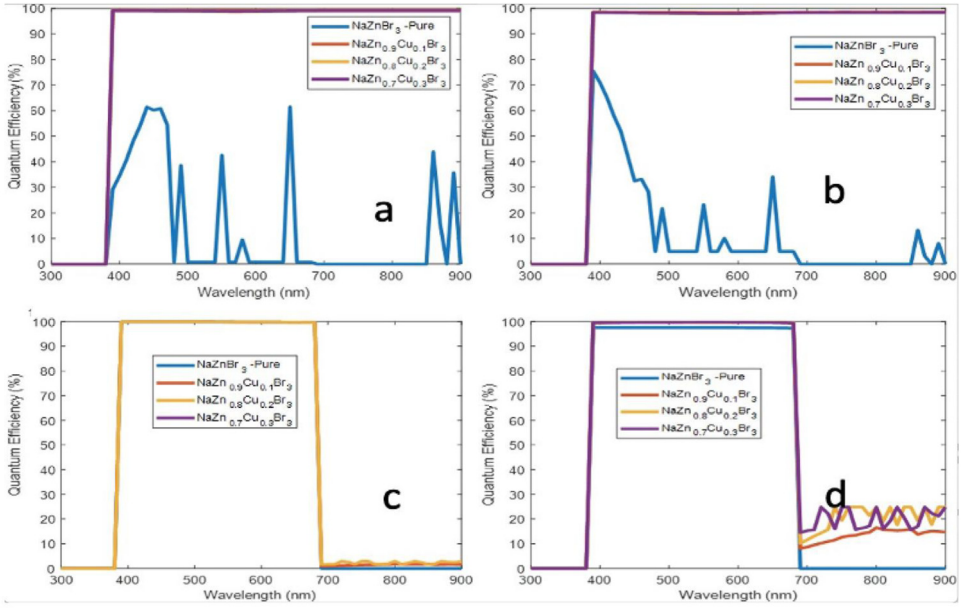

Fig. 5. Quantum Efficiency curves of simulated $NaZnBr_3$-based solar cells with and without copper dopants with perovskite thicknesses 100 μm, 10 μm, 1 nm, and 10 nm.

presence of the copper, which has its major peak between 330 nm and 700 nm (Ramyadevi et al., 2011). $NaZnBr_3$ has a higher band gap than CaZnBr3, however, that does not seem to be the cause of the lower efficiency in its pure state.

It is more likely due to its nature as a p–n heterojunction type semi-conductor as indicated in the Mott Schottky plot (Swain et al., 2018). The particular configuration of solar cell used here, which is the same for all the samples, may not be compatible with the unique properties of $NaZnBr_3$. However, doping does eliminate this property, and the efficiency improves dramatically with both copper and silver dopants, in agreement with the relevant graphs.

The morphology of the samples is presented in Figs. 7–9. The pure rice sample under the 300x magnification shows that there is low porosity with larger portion being smooth (Fig. 7). The fairly smooth surface as presented in higher magnification i.e., 1000x and 1500x are further evidence that majority of the particulate sizes is in the nanometer scale. This also makes it a good candidate to make the deliquescence $NaZnBr_3$ sample more rigid.

Fig. 8 shows the morphology of the mixture of rice powder and $NaZnBr_3$. It is observed that the coloration as well as the porosity increased due to the inherent properties of the perovskite. Also, the glittering surface and its cracks reveal the viability of this

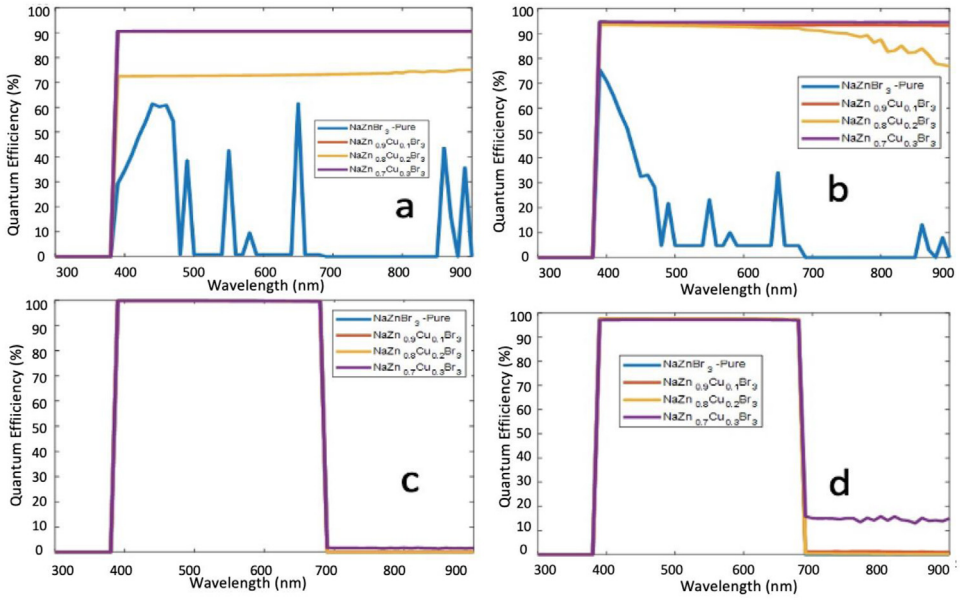

Fig. 6. Quantum Efficiency curves of simulated $NaZnBr_3$-based solar cells with and without Silver dopants with perovskite thicknesses 100 μm, 10 μm, 1 nm, and 10 nm.

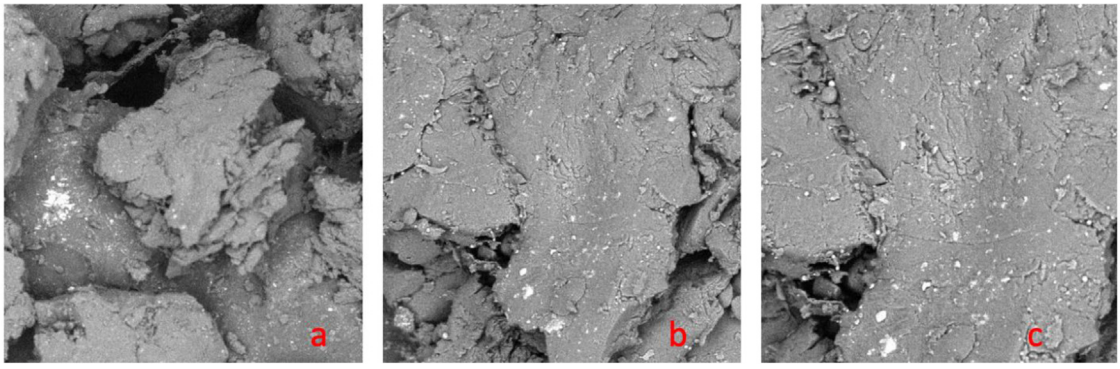

Fig. 7. Morphology of the rice powder (a) 300x magnification (b) 1000x magnification (c) 1500x magnification.

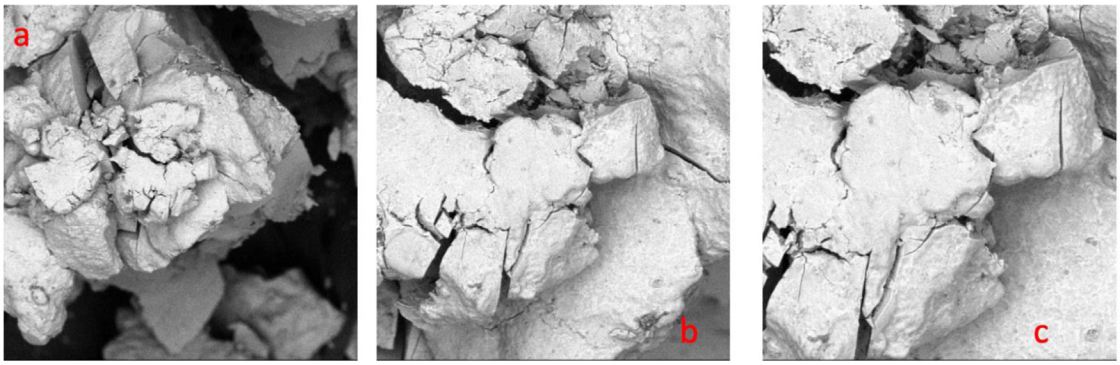

Fig. 8. Morphology of the rice powder + $NaZnBr_3$ (a) 300x magnification (b) 1000x magnification (c) 1500x magnification.

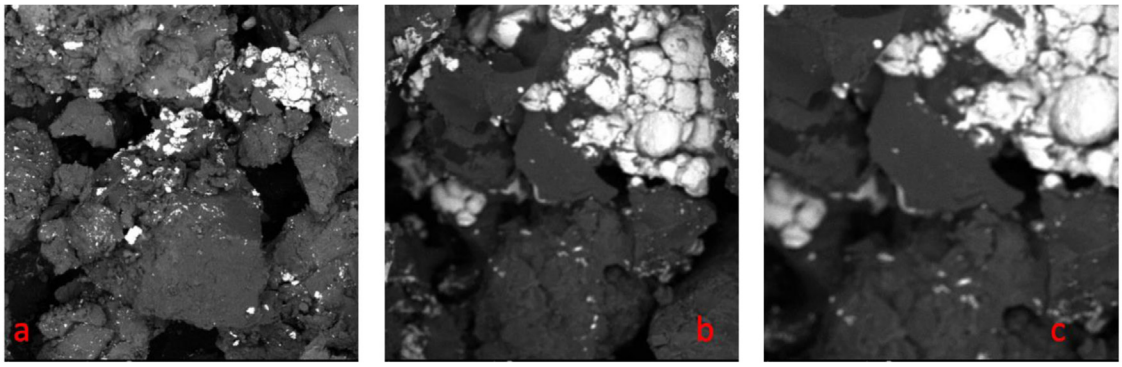

Fig. 9. Morphology of the rice powder + $NaZn_{0.7}Ag_{0.3}Br_3$ (a) 300x magnification (b) 1000x magnification (c) 1500x magnification.

compound to be commercially shaped to varying sizes according to photovoltaic module designs. The rigidity of the material via the addition of the rice powder to overcome the deliquescence nature of the $NaZnBr_3$ compound is promising physically.

Fig. 9 presents the morphology of the mixture of rice powder and $NaZn_{0.7}Ag_{0.3}Br_3$. Recall that in Table 3, $NaZn_{0.7}Ag_{0.3}Br_3$ was reported to have the highest efficiency which itself is a breakthrough in field of inorganic lead-free perovskite. The morphology was investigated to understand why it showed significantly higher efficiency compared its parent material i.e. $NaZnBr_3$. It is observed that the coloration as well as the porosity increased due to the inherent properties of the doped perovskite i.e., $NaZn_{0.7}Ag_{0.3}Br_3$. Unlike the parent material i.e., $NaZnBr_3$, the coloration is the evidence of formation of layer as reported by Brammertz et al. (2013). Under higher magnification, a whitish particulate was observed which may be the silver. The spread and localization of the whitish particulate are evidence that the lattice modification was such that will permit electron mobility. Hence, the morphology of the material further validates the theoretical calculation using SCAPS-1D.

The crystallographic structure of the materials was investigated as shown in Fig. 10. The XRD measurement was carried out using the XRD Rigaku D/Max-IIIC model with generator tension and current given as 40 kV and 20 mA respectively. The scanning angle ranges from 0–66.68°. Under a continuous scan technique with a maximum intensity of 1400cps, nine peaks were discovered and adequately labeled as presented in Fig. 10(a). The typical rice powder is highly oxidized as presented in Fig. 10(a). The peaks had the following planes i.e., (100), (110), (111), (200), (210), (220), (300), (310), and (211).

Fig. 10(b) shows the crystallographic structure of the mixture of rice powder and NaZnBr 3. Nine peaks were also obtained with same planes mentioned in Fig. 10(a). However, it is seen that the spaces within each peak and re-arrangement of the planes are evidences that the layers inherent in the perovskite were not altered even when it is padded with the rice powder. Literature has revealed that aside the high carbohydrate and protein content, the mineral contents is considerably low (Yoshihashi et al., 2004; Yadav et al., 2007). Hence, the influence of the rice powdered on the crystal structure of the enhanced novel perovskite is insignificant.

Fig. 10(c) shows the crystallographic structure of the mixture of rice powder and $NaZn_{0.7}Ag_{0.3}Br_3$. Nine peaks were also obtained with same planes mentioned in Fig. 10(a) and 10(b). However, the structural arrangement of the compound was like its parent material i.e. $NaZnBr_3$. From the idea that each chemical compound or phase reflects X-rays slightly differently and so has a different diffraction pattern, the impact on the sites can be inferred. Juxtaposing Fig. 10(b) and (c), the 'A' site can be identified by the planes (100), (110), and (111). The difference between both samples the prominence of plane (211) and relegations of planes (210) and (310). These scenario are evidence that only the 'B' sites that were doped as presented in the stoichiometry.

In other words, the crystallographic and microstructural structure of the perovskite plays a significant role in the optimization or modification of the efficiency of the novel $NaZnBr_3$ perovskite.

4. Conclusion

This study revealed that structural modifications of perovskite using Copper and Silver dopants can be used as a unique technique for enhancing the efficiency of $NaZnBr_3$. The optical characterization carried out using Ultraviolet–Visible (UV–VIS) spectroscopy revealed a band gap of 3.1 eV. The electronic characterization using SCAPS-1D showed that $NaZnBr_3$ had an efficiency of 0.88% at 100 μm. This efficiency improves to 9.33% with silver additive with a bandgap of 1.65 eV. The flat-band potential indicates a p–n type semiconductor, fit for heterojunction solar cells, however this property is removed by doping. The external quantum efficiency shows an increase with doping and implies better stability of the doped $NaZnBr_3$. Silver is also revealed as a better dopant than Copper as it gives the higher efficiency. In other words, the crystallographic and microstructural structure of the perovskite plays a significant role in the optimization or modification of the efficiency of the novel $NaZnBr_3$ perovskite. There were significant limitations in the study which includes the experimental determination of the efficiency of the novel perovskite in pure sample and when mixed with rice. It is recommended that $NaZnBr_3$ be researched further using different synthetic routes. Also, the experimental determination of the efficiency of the novel perovskite in pure sample and when mixed with rice should be researched further.

CRediT authorship contribution statement

Moses E. Emetere: Designed, Data curation of SEM and XRD and partly written. **Oluwaseyi O. Bello:** The curation of the data (UV and SCAP 1D), Part write-up. **S.A. Afolalu:** The part write-up done.

Declaration of competing interest

The authors declare that they have no known competing financial interests or personal relationships that could have appeared to influence the work reported in this paper.

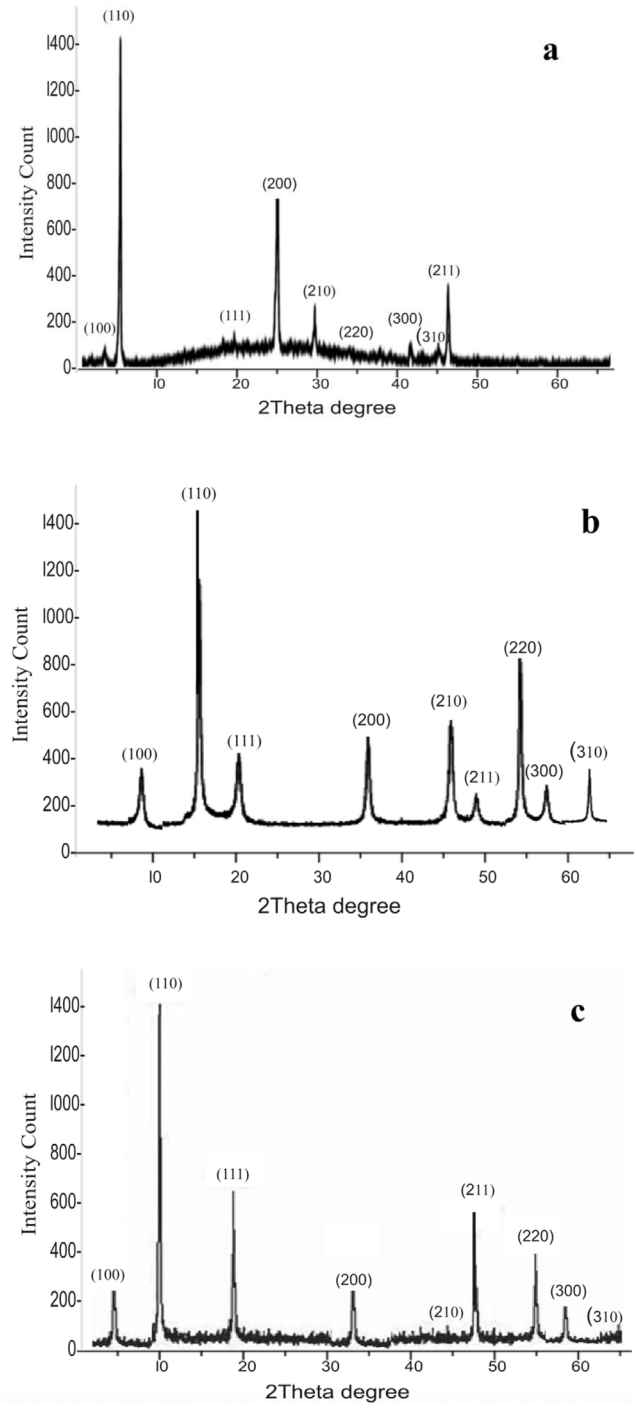

Fig. 10. The crystallographic structure of (a) rice powder (b) $NaZnBr_3$ (c) $NaZn_{0.7}Ag_{0.3}Br_3$.

References

Ahmed, M.I., Habib, A., Javaid, S.S., 2015. Perovskite solar cells : Potentials, challenges, and opportunities, vol.2015. 592308.

Brammertz, G, Buffière, M, Oueslati, S, ElAnzeery, H, Ben Messaoud, K, Sahayaraj, S, Köble, C, Meuris, M, Poortmans, J., 2013. Characterization of defects in 9.7% efficient Cu_2 Znsnse$_4$-CdS-ZnO solar cells. Appl. Phys. Lett 103, 163904.

Chen, M., et al., 2019. Highly stable and efficient all-inorganic lead-free perovskite solar cells with native-oxide passivation. Nat. Commun. 10, 16. http://dx.doi.org/10.1038/s41467-018-07951-y, In this issue.

Dengler, S., Kübel, C., Schwenke, A., Ritt, G., Eberle, B., 2012. Near- and off-resonant optical limiting properties of gold–silver alloy nanoparticles for intense nanosecond laser pulses. J. Opt. 14 (7), 075203. http://dx.doi.org/10.1088/2040-8978/14/7/075203.

Elumalai, N.K., Mahmud, A., Wang, D., Uddin, A., 2016. Perovskite solar cells. Prog. Adv. 9 (11), 861. http://dx.doi.org/10.3390/en9110861.

Greul, E., Petrus, M., Binek, A., Docampo, P., Bein, T., 2017. Highly stable, phase pure Cs2AgBiBr6 double perovskite thin films for optoelectronic applications. J. Mater. Chem. A 5 (37), 19972–19981. http://dx.doi.org/10.1039/c7ta06816f.

Igbari, F., Wang, R., Wang, Z.K., Ma, X.J., Wang, Q., Wang, K., Zhang, Y., Liao, L., Yang, Y., 2019. Composition stoichiometry of Cs 2 AgBiBr 6 films for highly efficient lead-free Perovskite solar cells. Nano Lett. 19 (3), 2066–2073. http://dx.doi.org/10.1021/acs.nanolett.9b00238.

Niemegeers, A., Burgelman, M., 1996. Numerical modelling of ac-characteristics of cdte and cis solar cells. In: Proc. 25nd IEEE Photovoltaic Specialists Conference, Vol.90. pp. 1–904.

Rahman, S.I., Faisal, S., Ahmed, S., Dhrubo, T.I., 2018. A comparative study on different HTMs in perovskite solar cell with ZnOs electron transport layer. In: 5th IEEE Region 10 Humanitarian Technology Conference 2017. Institute of Electrical and Electronics Engineers Inc., pp. 546–550. http://dx.doi.org/10.1109/R10-HTC.2017.8289019.

Rahman, M.S., Miah, S., Marma, M.S.W., Sabrina, T., 2019. Simulation based investigation of inverted planar perovskite solar cell with all metal oxide inorganic transport layers. In: 2nd International Conference on Electrical. In: Computer and Communication Engineering, ECCE 2019, Institute of Electrical and Electronics Engineers Inc, http://dx.doi.org/10.1109/ECACE.2019.8679283.

Ramyadevi, J., Jeyasubramanian, K., Marikani, A., Rajakumar, G., Rahuman, A.A., Santhoshkumar, T., Marimuthu, S., 2011. Copper nanoparticles synthesized by polyol process used to control hematophagous parasites. Parasitol. Res. 109 (5), 1403–1415. http://dx.doi.org/10.1007/S00436-011-2387-3.

Roman-Vazquez, M., Vidyasagar, C., Munoz-Flores, B., Jimenez-Perez, V., 2020. Recent advances on synthesis and applications of lead- and tin-free Perovskites. J. Alloys Compd. 835, 155112. http://dx.doi.org/10.1016/j.jallcom.2020.155112.

Roy, A., Ghosh, A., Bhandari, S., Sundaram, S., Mallick, T.K., 2020. Perovskite solar cells for BIPV application: a review, vol.10. (7), p. 129.

Sahli, F., Werner, J., Kamino, B.A., Bräuninger, M., Monnard, R., Paviet-Salomon, B., Ballif, C., 2018. Fully textured monolithic perovskite/silicon tandem solar cells with 25.2% power conversion efficiency. Nature Mater. 17 (9), 820–826. http://dx.doi.org/10.1038/s41563-018-0115-4.

Shao, Z., Mercier, T. Le, Madec, M.B., Pauporté, T., 2018. AgBi 2 I 7 layers with controlled surface morphology for solar cells with. Mater. Lett. 221, 135–138. http://dx.doi.org/10.1016/j.matlet.2018.03.085.

Swain, G., Sultana, S., Moma, J., Parida, K., 2018. Fabrication of hierarchical two-dimensional MoS2 nanoflowers decorated upon cubic CaIn2S4 microflowers: Facile approach to construct novel metal-free p-n heterojunction semiconductors with superior charge separation efficiency. Inorg. Chem. 57 (16), 10059–10071. http://dx.doi.org/10.1021/acs.inorgchem.8b01221.

Usikalu, M.R., Przybyłowicz, W.J., Mtshali, C., Babarimisa, I.O., 2017. Elemental analysis of commonly consumed rice in Nigeria using PIXE technique. J. Inform. Math. Sci. 9 (2), 417–422.

Wang, M., Zeng, P., Bai, S., Gu, J., Li, F., Yang, Z., Liu, M., 2018. High-quality sequential-vapor-deposited Cs 2 AgBiBr 6 thin films for lead-free perovskite solar cells. Solar RRL 2 (12), 1800217. http://dx.doi.org/10.1002/solr.201800217.

Wannee, Srinuttrakul, Arporn, Busamongkol, 2014. Elemental analysis of brown rice by inductively coupled plasma atomic emission spectrometry and instrumental neutron activation analysis. Energy Procedia 56, 85–91.

Yadav, R.B., Khatkar, B.S., Yadav, B.S., 2007. Morphological, physicochemical and cooking properties of some Indian rice (oryza sativa l.) cultivars. J. Agric. Technol. 3 (2), 203–210.

Yoshihashi, T., Nguyen, T.T.H., Kabaki, N., 2004. Area dependency of 2-acetyl-1-pyrroline content in an aromatic rice variety, Khao Dawk Mali 105. Jpn. Agric. Res. Quant. 38 (2), 105–109.

Zhang, Z., Wu, C., Wang, D., Zhang, Q., Guo, X., Lao, Y., Qu, B., Xiao, L., Chen, Z., 2020. Efficient non-lead double perovskite solar cell with multiple hole transport layers. ACS Appl. Energy Mater. 10, 9594–9599. http://dx.doi.org/10.1021/acsaem.0c01066.

Zhao, D., Wang, B., Liang, C., Liu, T., Wei, Q., Wang, S., Wang, K., Zhang, Z., Li, X., Peng, S., Xing, G., 2020. Facile deposition of high-quality Cs2AgBiBr6 films for efficient double perovskite solar cells. Sci. China Mater. 63 (8), 1518–1525. http://dx.doi.org/10.1007/s40843-020-1346-0.

Zhou, D., Zhou, T., Tian, Y., Zhu, X., Tu, Y., 2018. Perovskite-based solar cells : Materials, methods, and future perspectives. J. Nanomater. 2018, 15.